AN IMPROVED DRAG MODEL FOR CBERS ORBIT DETERMINATION AND PROPAGATION

Hélio Koiti Kuga[(1)], **Valdemir Carrara**[(2)], **and Luiz Arthur Gagg Filho**[(3)]
[(1)(2)] *INPE - National Institute for Space Research, Av. dos Astronautas, 1758 São José dos Campos, SP - 12227010 Brazil,55-12-3208-6183, valdemir.carrara@inpe.br, helio.kuga@inpe.br*
[(3)] *ITA – Technological Institute of Aeronautics, Praça Marechal-do-Ar Eduardo Gomes, 50 São José dos Campos, SP 12228900 Brazil, 55-12-3947-5732, luizarthur.gagg@gmail.com*

Abstract: *The CBERS-2 was one of the satellites of CBERS (China-Brazil Earth Resources Satellite) series, launched in 2003. With an altitude of 778 km, its orbit is mainly perturbed by the atmospheric drag. The current model for orbit propagation, used by the CBERS Control Center at the National Institute for the Space Research (Brazil), considers a constant value for the drag coefficient. In fact, the drag was estimated during orbit acceptance phase, which resulted 2.5. This model was then frozen and it is still being used for orbit determination and propagation. However it is known that the drag depends on several parameters, in particular the Mach number, the surface temperature and accommodation coefficients. In this work it is considered a model for the drag forces on CBERS based on the kinetic theory of gases. The algorithm considers that the external satellite geometry is described by a boundary representation (b-reps) similar to that used in computer graphics such as OpenGl. Satellite surface is divided in a finite number of triangles, each one described by its vertex coordinates. Geometry is stored in an ASCII file using a subset of NASTRAN commands for mesh description. Once the mesh is stored in memory, the forces and torques acting on the satellite (drag and solar radiation pressure) can be calculated by integrating it over the external surface. The computation time for drag forces is, of course, several times higher than the constant coefficient model. The main goal of this work is to compare this model with the constant drag coefficient results, to retrieve eventual discrepancies and to check the orbit deviation in both cases. The atmospheric properties were obtained from an analytical model proposed by Mueller, based on the Jacchia's 1977 model. The results have shown that there were some significant improvements in orbit prediction, although not always.*

Keywords: *Orbit determination, Satellite drag, Aerodynamic forces, Kinetic theory of gases.*

1. Introduction

Besides CBERS-1 (launched in 1999) and 2 (launched in 2003), CBERS-2B was the latest satellite of CBERS (China-Brazil Earth Resources Satellite) series, launched in 2007. The follower CBERS-3 was lost due to launcher failure, and CBERS-4 is scheduled to be launch late in 2014. CBERS satellites have polar sun-synchronous orbit with an altitude of 778 km, Equator crossing at 10:30 AM in descending direction, frozen eccentricity and perigee at 90 degrees, and provides global coverage of the world every 26 days. With such characteristics its orbit, besides gravitational forces, is mainly perturbed by the atmospheric drag and solar radiation pressure, amongst others (third body attraction, tides, etc.). However drag perturbation has shown to be most difficult to model in view of the need of accuracy for long lasting predictions. The current model for orbit propagation, used by the CBERS Control Center at the National Institute for the

Space Research (Brazil), considers a constant value for the drag coefficient. This coefficient was estimated just after orbit injection, which resulted a mean value of 2.5. This constant drag model is still being used for orbit determination and propagation at the INPE´s control center. Nevertheless the atmospheric drag depends on a multitude of different parameters with several sources, in particular the Mach number, the surface temperature and accommodation coefficients. In this work it was adopted a model for the drag forces based on the kinetic theory of gases, as proposed by [1]. The method models the satellite geometry by means of planar surfaces defined by their area and normal or, equivalently, by their vertexes. Curved geometries can be described by a finite number of triangles or quadrilaterals. The geometry can be informed to the computation package by an ASCII file using a subset of NASTRAN commands for the mesh description or directly by programming code. The mesh is then read by some package procedures and stored in memory, for later integration of the forces and torques over the external surface. The expected integration time is higher than the computation time of the constant coefficient model, but it is acceptable since the expected gain of the orbit determination residuals shall be low. The main goal of this work is to compare this model with the quasi-constant drag coefficient results from the control center, in a long term basis, for instance a couple of months at least (between maneuvers). Therefore eventual discrepancies can be retrieved and the orbit elements deviation can be promptly analyzed. The atmospheric properties were obtained from an analytical model proposed by Mueller [2] based on the Jacchia's 1977 model [3]. Indeed any density model could be used as reference to draw the essential conclusions. Since computing time is not a very constraining requirement nowadays, it is expected that either the variable drag and radiation pressure models for force computation or a corresponding suitable empirical parameterization can be successfully applied in the upcoming CBERS missions. In short, this paper presents a comparison between the current orbit determination and propagation procedures of CBERS (China-Brazil Earth Remote Sensing) satellite, mostly based on a fixed drag coefficient, and a model that uses the kinetic theory of gases to compute the forces and torques on a satellite with a given geometry. A similar approach is used regarding the satellite geometry description for the solar radiation pressure. The main goal was to retrieve eventual discrepancies between models, and to check the orbit deviations in such cases. The results have shown that there were some significant improvements in orbit prediction, when applied for long arcs (e.g. some months).

2. Environmental perturbation models

A precise orbit determination algorithm relies always on the orbit dynamics, which, in turn, depends on how accurate is the orbit perturbation model. There are several sources of orbit and attitude perturbations in the space environment acting from low to high altitude orbits and also in the interplanetary ones. They can be grouped in gravitational, electromagnetic and surface interaction sources, with intensities extending from 10^{-3} N (it depends on the spacecraft size, actually) down to 10^{-30} N and beyond. Of course, such a small magnitude sources can be detected only in satellites with particular shapes where all the major effects are cancelled or simply not applicable for that orbit. For low Earth orbit where most satellites are, the main perturbation is the drag or aerodynamic force, followed by the solar radiation pressure, if one does not take into account the orbit distortion due to the non-uniformity of the Earth's gravitational field. Gravity gradient torque plays an important role in asymmetric satellites, but only in attitude. Also a source of torques is the interaction of the magnetic field of the satellite

generated by unbalanced electrical currents or by the on-board magnetic materials with the Earth's magnetic field. Finally, mutual interaction between an electrically conducting satellite with the ionosphere and the geomagnetic field produces several small effects that can be neglected in most satellites. They are also particularly difficult to model for non-symmetric shaped satellites. Below approximately 700 km altitude the drag is the most significant perturbation on orbits, whereas solar radiation pressure are predominant above this altitude and on geo-synchronous orbits [4].

2.1. Atmospheric drag modeling

Although a constant drag coefficient is still employed for orbit determination, i.e., for calculating the orbit elements or ephemeris based on satellite position measurements, it has been demonstrated that the interaction of the exosphere molecules with the satellite surface is a complex phenomenon which can be modeled by the kinetic theory of gases (besides some empirical models) [1], [5] and [6]. In order to obtain the aerodynamic force the velocity distribution function of a gas shall be used:

$$f = \frac{\rho_o}{m}\left(\frac{m}{2\pi\, k\, T}\right)^{3/2} \exp\left[-\frac{m}{2kT}(\mathbf{v}-\mathbf{v}_o)^2\right], \tag{1}$$

for a monomolecular gas in thermal equilibrium and not subjected to a gravitational field. The above expression gives the probability to find a molecule with velocity between **v** and **v** + d**v** with molecular mass m, in a gas with density ρ_o, with mean flux velocity $\mathbf{v}_o$ with respect to a reference frame, and absolute temperature T (k is the Boltzmann constant). The velocity distribution function can be employed to compute the momentum transferred by the gas molecules that strikes a static surface coming from a given direction, as depicted in Fig. 1. To compute the force exerted by the gas on the surface it is assumed [1] that the momentum exchanged by the molecules both in normal and tangential directions does not depend of the molecule velocity or direction of incidence. A single coefficient seems to be inaccurate to describe the gas surface interaction, and so a normal and tangential transfer momentum coefficients were introduced by [1]:

$$\sigma_n = \frac{p_i - p_r}{p_i - p_w}, \text{ and } \sigma_t = \frac{\tau_i - \tau_r}{\tau_i}, \tag{2}$$

that give, respectively, the momentum exchanged in normal and tangential directions. p_i and p_r are the momentum carried by the incident and reflected molecules in the surface normal direction, respectively, while τ_i and τ_r are the momentum in tangential direction of the incident and reflected molecular flux. p_w stands for the momentum carried out by the reflected molecules in case they arise from the surface with thermal equilibrium with it, at the same surface temperature. For elastic collision both σ_n and σ_t are close to zero, and for a fully interaction, where the reflected molecules are in a maxwellian equilibrium with null velocity and at same surface temperature, the coefficients tend to unit.

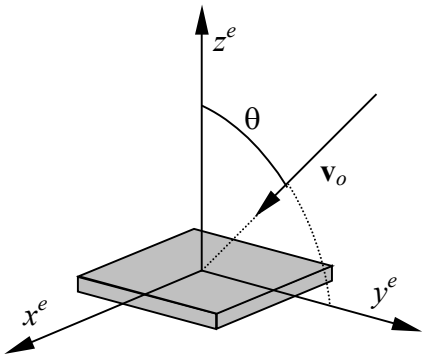

Figure 1. Gas flux hits the surface coming from a known direction.

Now the aerodynamic pressure on a small flat surface can be derived, and results, respectively in normal and incident directions:

$$p_k = -\frac{\rho_i\, v_o^2}{2}\frac{1}{s^2}\left\{\left[\frac{2-\sigma_n-\sigma_t}{\sqrt{\pi}}\, s\cos\theta + \frac{\sigma_n}{2}\sqrt{\frac{T_w}{T_i}}\right]\exp\left(-s^2\cos^2\theta\right) + \right.$$
$$\left. + \left[(2-\sigma_n-\sigma_t)\, s^2\cos^2\theta + 1 - \frac{\sigma_n}{2} + \frac{\sigma_n}{2}\sqrt{\pi}\sqrt{\frac{T_w}{T_i}}\, s\cos\theta\right]\left[1+\operatorname{erf}\left(s\cos\theta\right)\right]\right\}, \tag{3}$$

$$p_u = \frac{\rho_i\, v_o^2}{2}\frac{\sigma_t}{s\sqrt{\pi}}\left\{\exp\left(-s^2\cos^2\theta\right) + \sqrt{\pi}\, s\cos\theta\left[1+\operatorname{erf}\left(s\cos\theta\right)\right]\right\}, \tag{4}$$

where ρ_i is the local atmospheric density, T_w is the surface absolute temperature, T_i is the incident flux absolute temperature, erf(·) is the error function and θ is the incident angle ($\cos\theta = -\mathbf{n}\cdot\mathbf{u}$, where $\mathbf{u}$ is the incident unit vector: $\mathbf{u} = \mathbf{v}_o / v_o$). The speed ratio s is the ratio between the flux mean velocity, $\mathbf{v}_o$, and the most probable velocity of the molecules, given by

$$s = \left|\mathbf{v}_o\right|\sqrt{\frac{m}{2k\, T_i}}, \tag{5}$$

The aerodynamic pressure shall be integrated over the external satellite surface, so as to give the force acting on the satellite:

$$\mathbf{f}_{aer} = \int_{A_{ext}} \left(p_k\, \mathbf{n} + p_u\, \mathbf{u}\right) dA, \tag{6}$$

The integration shall be performed over all the external satellite surfaces, but care must be taken because only convex shaped satellites are valid. In fact, since the distribution function of the reflected beam differs from the incident flux due to thermal accommodation, double or triple molecule collision with the satellite are not taken into account. Normally this effect can be neglected and the integration error for concave shaped satellites is small. The "shadowing" effect, where a part of the satellite like an antenna or panel occludes another part in the mean

flux direction, makes the integral differ from the correct one [7]. Although the molecules strike the satellite coming from any direction, the main contribution to the force are the ones in the flux direction. For convex satellites with constant surface properties (temperature and momentum coefficients) and simple geometry, like sphere, cylinder, cone and box, the aerodynamic force (and, eventually, also the torque) can be analytically integrated over the external surface [8], [9], [10], [11], [12]. Unfortunately, experimental data about the momentum transfer coefficients are scarce. They seem to show, however, that the reflection tends to be diffuse (σ_n and σ_t close to unit) even for highly polished surfaces [1]. In view of the lack in the momentum coefficient data, this work proposes to manually adjust these coefficients to match the satellite orbit decay, instead of the drag coefficient alone. This procedure has the advantage that, unlike the drag coefficient estimation, it produces a more accurate fitting since the actual drag force varies with the local atmospheric density, temperature, satellite velocity and attitude. Notice that this approach does not need explicit computation of the drag coefficient C_d as is usually done in most numerical orbit computations.

The thermosphere properties were computed by the Jacchia-Lineberry [2] model and adapted to the Jacchia-77 thermospheric model [3], although several other models are available for orbit integration in the simulation package [13]. The thermospheric models depend on the mean and observed Solar Flux at 10.7 cm wavelength at a given date. The flux varies with solar activity, which presents a 10.6 years cycle. During solar storms, the solar wind deflects the geomagnetic field, which causes a significant heating in the thermospheric molecules. This effect is named geomagnetic activity and is measured by geomagnetic observatories spread around the world. Both the solar flux and geomagnetic activity were compiled and stored in a single file, together with the flux mean values necessary to feed the models, and are freely available [13].

2.2. Solar radiation modeling

The solar radiation force can be modeled in a similar way. The incidence of Sun light on a satellite produces a force due to the exchange of momentum between the light photons and the surface [12], [14], and [15]. At the Earth distance from Sun, the pressure of the sunlight over a flat plane of 1 square meter is approximately 4.5 μN. The pressure at a distance R in astronomical units from Sun is computed by

$$p = \frac{S_o}{c}\left(\frac{1}{R}\right)^2, \tag{7}$$

where S_o is the solar power at 1 astronomical unit distance from Sun (S_o = 1353 W/m^2), and c is the light speed. The force on a flat plane is obtained by assuming that the incident beam can be reflected partially in the specular direction, partially scattered by the surface, and partially absorbed or transmitted. Two coefficients are necessary to describe the reflection phenomenon: the specular fraction, e, and the diffuse fraction, δ. If α is the absorbed and transmitted fraction, the coefficients shall obey $e + \delta + \alpha = 1$. The absorbed fraction heats the surface and it begins to emit diffuse radiation according to the Stefan-Boltzmann law:

$$S_i = \varepsilon\, \sigma\, T_w^4, \tag{8}$$

where S_i is the emitted power, ε is the surface emissivity, σ is the Stefan-Boltzmann constant (σ = 5,667 10^{-8} W/m^2 K^4) and T_w is the surface absolute temperature. By assuming that the reflection model follows the Lambert cosine law, the force components in normal, **n,** and incident, **s**, directions can be obtained, resulting

$$p_n = -p \cos\eta \left[2\, e \cos\eta + \frac{2}{3}\delta \right] - \frac{2}{3}\frac{\sigma}{c}\varepsilon\, T_w^4 , \tag{9}$$

$$p_s = p \cos\eta\,(1-e) \ , \tag{10}$$

where η is the light incidence angle with respect to the surface normal ($\cos\eta = -\mathbf{n}\cdot\mathbf{s}$). The elementary solar pressure force shall be integrated over the external surface in a similar way to that employed in the aerodynamic force computation:

$$\mathbf{f}_{srp} = \int_{A_{ext}} \left(p_n\, \mathbf{n} + p_s\, \mathbf{s} \right) dA , \tag{11}$$

and, as before, mutual shadowing shall be avoid in the integration. That excludes, of course, the concave satellites, although the error committed when the shadow is neglected depends on the satellite geometry and is, normally, small. Therefore, only external surfaces that are exposed to the sunlight shall be considered in the integration. They must obey the condition $\cos\eta > 0$, otherwise they shall be omitted from computation, except by the emitted parcel. The radiation force can then be expressed as

$$\mathbf{f}_{srp} = \begin{cases} \int_{A_{ext}} \left(p_n\, \mathbf{n} + p_s\, \mathbf{s} \right) \mathrm{d}A, \ \text{if } \cos\eta > 0 \\ -\frac{2}{3}\frac{\sigma}{c}\varepsilon \int_{A_{ext}} T_w^4\, \mathbf{n}\, \mathrm{d}A, \ \text{if } \cos\eta \le 0 \end{cases} , \tag{12}$$

If the external surface temperature T_w is constant all over the satellite, then it can be shown that the resultant reemission radiation force is null and can be removed from integration in order to speed up calculations. Notice that, similarly to the drag modeling, such approach precludes explicit computation of the C_r (solar radiation pressure coefficient). However in this case one can include the C_r as a parameter to be fitted in the orbit determination system, and the difference between the estimated C_r and the nominal C_r = 1 indicates the adequacy of the proposed modeling. Although not included in this work, the indirect radiation pressure could easily be implemented, however making the necessary arrangements to integrate over the whole Earth surfaces contributing to the albedo effect [16].

2.3. Satellite geometry

The satellite geometry can be described by a boundary-representation similar to that one employed in computer graphics or finite element theory. A set of C++ functions to compute the environmental perturbations was implemented and used in this work to compare the simulated

with the orbital data for the satellite CBERS. The package (EDM – Environmental Disturbance Models) can accept the geometry in several different ways, like size and normal direction, triangles, quadrilaterals, mesh, cylindrical, spherical, conical, box, and any combination of these geometries, besides a geometry description file for plane elements only [17]. The description file adopts a structure similar to NASTRAN, composed by commands that define the vertex table (GRID), and the polygon table (CTRIA3 for triangles and CQUAD4 for quadrilaterals). A MATERIAL command was introduced so as to define the surface properties like transfer momentum and reflection coefficients, together with a BODYAP command to set if a given polygon is fixed to the body frame or is fixed to an appendage, like a solar panel, for instance. This arrangement allows the program user to effectively rotate (or translate) each appendage at run time, in a similar way to that of a real tracking solar panel, and therefore increases the accuracy and model fidelity. Although only NASTRAN geometry description file is supported by the EDM package, any other boundary-rep can be converted to it. In this case any 3D editing program with ASCII exporting capability can be used to generate the satellite geometry. The geometry of CBERS, shown in Figure 2, was manually inserted into the NASTRAN data file.

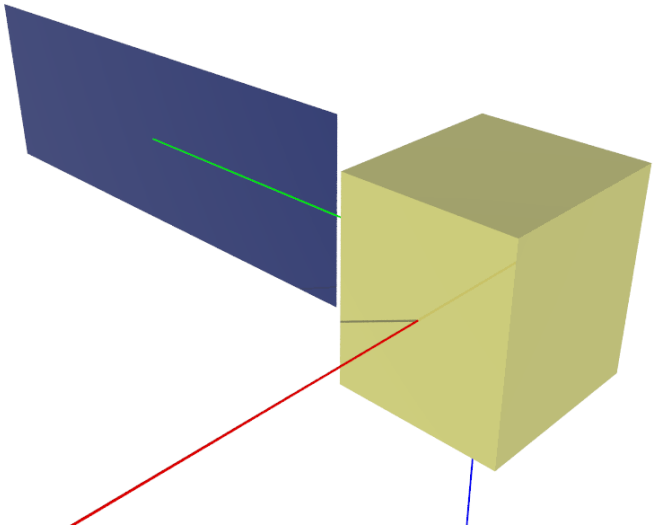

Figure 2. CBERS simplified geometry, with only 8 quadrilateral polygons.

The EDM package includes, besides the aerodynamic and solar radiation forces and torques, the gravity gradient and magnetic torques, the Sun and Moon gravitational acceleration in an Earth orbit satellite, and the Earth's gravitational field up to order 2190 [18] and [19]. The complete model was used to adjust the CBERS parameters to comply with the observed orbital data. The results are report in next sections.

2.4. Other perturbations

Any Earth artificial satellite is subject to attraction by the non-central gravitational field and suffers disturbances due to non-spherical and non-symmetrical distribution of Earth mass. The potential of the satellite relative to the unevenly distributed Earth mass is calculated in a generic form by:

$$V = \frac{GM_e}{r} \sum_{n=0}^{\infty} \sum_{m=0}^{M} \left(\frac{a}{r} \right)^n \left[\overline{C}_{nm} \cos m\lambda + \overline{S}_{nm} \sin m\lambda \right] \overline{P}_{nm} (\sin \psi), \tag{13}$$

where V is the potential, G is the universal gravitational constant, M_e is the Earth mass, M is the truncation index, r is the distance to body from the Earth center, a is the Earth equatorial radius, λ is the longitude of body, Ψ is the geocentric latitude of body, $\overline{P}_{nm}$ are the fully normalized Legendre polynomials of order n and degree m, and $\overline{C}_{nm}, \overline{S}_{nm}$ are the fully normalized spherical harmonics coefficients. In this work the standard forward-column implementation proposed by [18] to higher order and degree was coded, as described in [19], which showed its performance in computation of Earth orbits up to order 2159 and degree 2190, corresponding to EGM2008 model. It is preferred to reverse the order of computation of the summation on Eq. 13, where the outer loop in m is first computed. The summation in the geopotential is then rewritten as:

$$V = \frac{GM}{r} + \frac{GM}{r} \sum_{m=0}^{M} \left[\cos(m\lambda) \sum_{n=\mu}^{M} \left(\frac{a}{r} \right)^n \overline{C}_{nm} \overline{P}_{nm} (\theta) + \sin(m\lambda) \sum_{n=\mu}^{M} \left(\frac{a}{r} \right)^n \overline{S}_{nm} \overline{P}_{nm} (\theta) \right], \tag{14}$$

where $0^\circ \le \theta \le 180^\circ$ is the co-latitude, and defining the inner summation components by:

$$X_{mC} \equiv \sum_{n=\mu}^{M} \left(\frac{a}{r} \right)^n \overline{C}_{nm} \overline{P}_{nm} (\theta), \qquad X_{mS} \equiv \sum_{n=\mu}^{M} \left(\frac{a}{r} \right)^n \overline{S}_{nm} \overline{P}_{nm} (\theta), \tag{15}$$

$$\Omega_m \equiv \cos(m\lambda) X_{mC} + \sin(m\lambda) X_{mS}, \tag{16}$$

where μ is an integer that depends on m, the potential yields

$$V = \frac{GM}{r} + \frac{GM}{r} \sum_{m=0}^{M} \Omega_m, \tag{17}$$

The gradient of the potential is then obtained in terms of spherical coordinates λ, θ, r, and transformed to Cartesian coordinates. The implementation details can be found in [19]. The codes were tested up to order 2159 and degree 2190 without any noticeable flaw. Numerical degradation near the poles was expected, although up to 0.000001° of proximity to the pole, i.e. ±89.999999° latitude, no problems were reported.

The other major perturbation taken into account was the point mass attraction. The point mass models represent the gravitational effects of a third perturbing body such as the Sun and Moon. The acceleration due to point mass effects is modeled by:

$$\ddot{\mathbf{r}}_{pm} = \mu_p \left(\frac{\mathbf{r}_p - \mathbf{r}}{\left|\mathbf{r}_p - \mathbf{r}\right|^3} - \frac{\mathbf{r}_p}{\left|\mathbf{r}_p\right|^3} \right), \tag{17}$$

where μ_p is the gravitational coefficient (GM_p) of the perturbing body, and $\mathbf{r}_p$ is the inertial position vector of the perturbing body. The only third perturbing bodies considered are the Sun and the Moon, whose inertial coordinates are obtained analytically, with an accuracy of 10^{-3} degrees for the Sun and 10^{-2} degrees for the Moon.

3. Application Results

The CBERS-2 was one satellite of CBERS (China-Brazil Earth Resources Satellite) series, launched in 2003. The satellite orbit is designed to be a Sun-synchronous type with frozen orbit characteristics (frozen perigee at 90º and frozen eccentricity at 0.0011). Due to its nominal altitude of 778 km and inclination of 98.50435º (for sun-synchronicity) CBERS-2 is mostly perturbed by the atmospheric drag. However other perturbations may play important roles as far as long-term orbit accuracy is needed.

The Satellite Control Center (CCS) of INPE (Brazilian Institute for Space Research) is in charge for the station keeping activities of some satellites. The orbit determination system of CBERS-2 uses tracking data (ranging and Doppler data) of the ground station network to compute the orbit. The orbit determination is periodically performed every 2 or 3 days intervals (3 times a week) and includes the main orbital perturbations: geopotential, atmospheric drag, solar radiation pressure (direct and albedo), and Sun and Moon effects. Every orbit determination outputs also the orbit mean elements, which is recorded to the mission history files. Such orbit elements are used to feed the on-board orbit propagator and is accurate enough to 3 days without need of updating. The basic theory of [20] adapted to non-singular elements by [21] to frozen orbits is used to compute the mean frozen orbit elements.

Therefore the satellite CBERS-2 is used as the test case to validate the modeling proposed. It was selected an interval in which there were no orbit maneuvers, i. e. no orbit maintenance. The period of 2003-November-11 10:02:10 UTC to 2004-June-28 02:20:00 UTC (around 231 days) was selected due to the relatively smooth and moderate solar activity behavior and where the CCS control center did not perform any maintenance orbit maneuver. As reference data to orbit analysis the control center yielded the orbit mean elements corresponding to the 94 orbit determinations during that time span. Figure 3 shows the behavior of the mean semimajor axis and inclination spanning that interval. It can be seen that the semimajor axis and inclination decays correspond to 250m and 0.025º in 231 days.

Figure 4 shows the characteristics of the frozen orbit of CBERS-2, where the centroid of the eccentricity versus argument of perigee is 0.00116, 91.17º, which are slightly offset from the nominal 0.0011 and 90º.

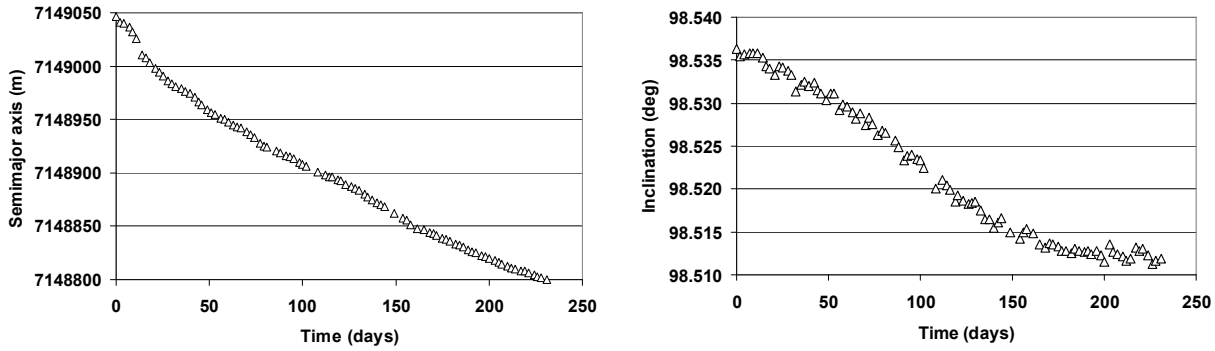

Figure 3. Mean semimajor axis and inclination computed by the Control Center

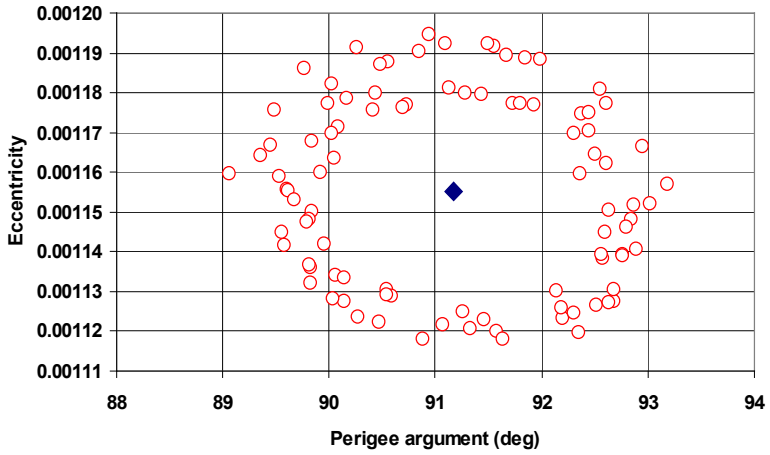

Figure 4. Mean eccentricity versus argument of perigee for the 231 days

The proposed models for atmospheric drag and radiation pressure were implemented and the orbit was integrated numerically for the whole span of 231 days. The numerical ODE (Ordinary Differential Equations) integrator Runge Kutta of order 4 with fixed step size of 10s was used to generate the osculating orbit. In all cases the geopotential model (EGM-2008) was set up to order and degree 50. The atmospheric properties were obtained from an analytical model [2], based on the Jacchia's 1977 model [3]. The solar activity data was taken from a database available to the software package. Both the transfer momentum coefficients for drag computation were fixed equal to unit, after adjustments made in order to fit the model to the mean orbit decay taken from the CBERS history file. The reflection coefficients, specular and diffuse, were initially chosen as $e = 0.8$ and $\delta = 0$ for both the satellite bus and solar array. However, from the simulated orbit, it became clear that the coefficients have minimum influence on orbital parameters, due to the small magnitude of the radiation forces compared to the drag. The coefficients were kept then equal to the previous values.

All the results were generated using an Intel Core i7-4500u processor, with RAM memory of 16GB, under 64 bits Windows 8.1 operating system, and the C++ compiler from Microsoft Visual Studio 2010 Version 10.030319.1. For a glimpse on the computer burden, Table 1 shows the CPU times when using the full numerical model (Geopotential 50x50, atmospheric drag,

radiation pressure, Sun-Moon attraction), and cases where the drag model was replaced by a simple model with fixed C_d, and the radiation pressure was also a model with fixed C_r. One concludes that the proposed drag model is more time consuming than the proposed radiation pressure model, and that the overhead with respect to the cannon ball models (fixed C_d or fixed C_r) is around 11%. Comparing with both fixed C_d and C_r models, the overhead is around 17%, which can be still considered affordable. At the end, for the sake of comparison, we included in Table 1 (last row) the CPU time when a higher order Runge-Kutta 7-8 (Fehlberg coefficients) was used. The time did not doubled, the overhead was around 35% (compare with first row). The results for both integrators (RK4 versus RK7, step-size of 10s) were quite similar differing at the end to the level of less than 10m, considered negligible when faced with the long integration time (231 days).

Table 1. CPU times

Model	CPU (s)	% overhead
Full	413.997	16.8
Full with $C_d = 2.0$	373.653	5.4
Full with $C_r = 1.5$	376.612	6.3
Full with $C_d = 2.0$ and $C_r = 1.5$	354.384	0
Full RKF78	537.376	51.6

For each orbit determination epoch from CCS (94 epochs) the Brouwer mean elements were computed from the numerically integrated osculating orbit. The formulation of [21] was employed, fitting at least 2 days of the osculating orbit around the corresponding epochs. That makes possible the comparison between the CCS and numerical mean elements for such long-term span.

3.1. Atmospheric Drag Model Results

In order to compare the results for the proposed drag model, the orbit was integrated for the 231 days including all other perturbations. For the sake of comparison the classical model of cannon ball results were also included. In this case the drag is modeled as an equivalent sphere with fixed C_d and area-over-mass ratio. However, the atmospheric density model [3] is being computed every step as before. Two cases were included: $C_d = 2.0$ (perfect sphere case) and $C_d = 2.5$ (nominal C_d of the control center). Figures 5 and 6 show the semimajor axis and inclination time history for different models of the atmospheric drag when compared to the control center (CCS) results. The "Num" stands for the full drag model as proposed herein, $C_d = 2.0$ and $C_d = 2.5$ means the cases where fixed C_d's are used.

In the computation by the numerical integrator it was adopted for both the normal and tangential transfer momentum coefficients the values 1.0. Such coefficients were fixed in order to obtain a manual fitting between the reference orbit and the numerically integrated orbit. Likewise the numerical orbit osculating elements were adjusted till the decay curves were close enough. It is realized in the orbital decay shown in Fig. 5 that all models (numerical and fixed C_d models) present different decay rates in some epochs, for instance around day 50 and again in the region near day 200. The only possible explanation for this difference is no doubt the discrepancy in the data values of the solar activity (solar flux and geomagnetic activity) used, which yields the

actual drag presented by the reference CCS orbit. Up to the moment it was not achieved a reasonable explanation for the fact however efforts are in course to obtain a conclusive and consistent answer. On the other hand all models presented good agreement with the reference with respect to orbit inclination, as shown in Fig. 6.

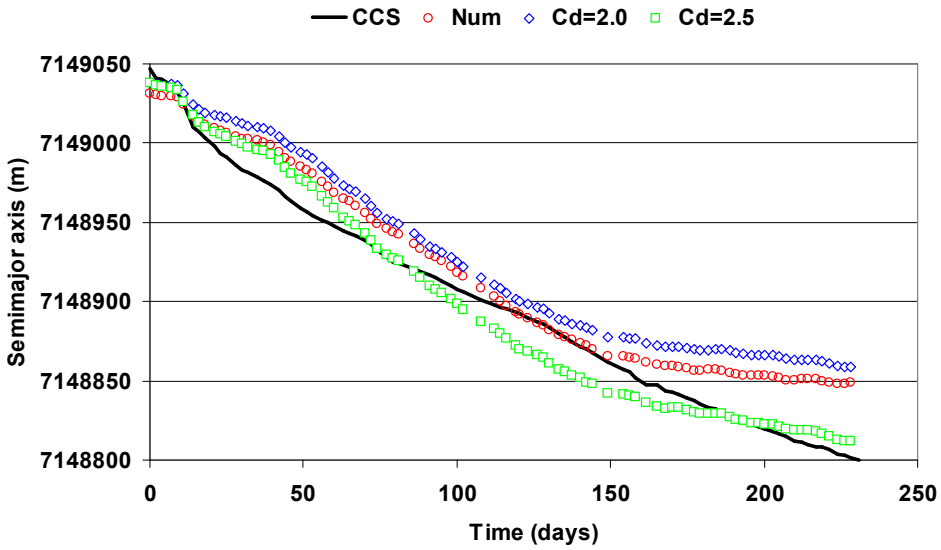

Figure 5. CBERS semimajor axis computed by CCS and numerical integration of drag.

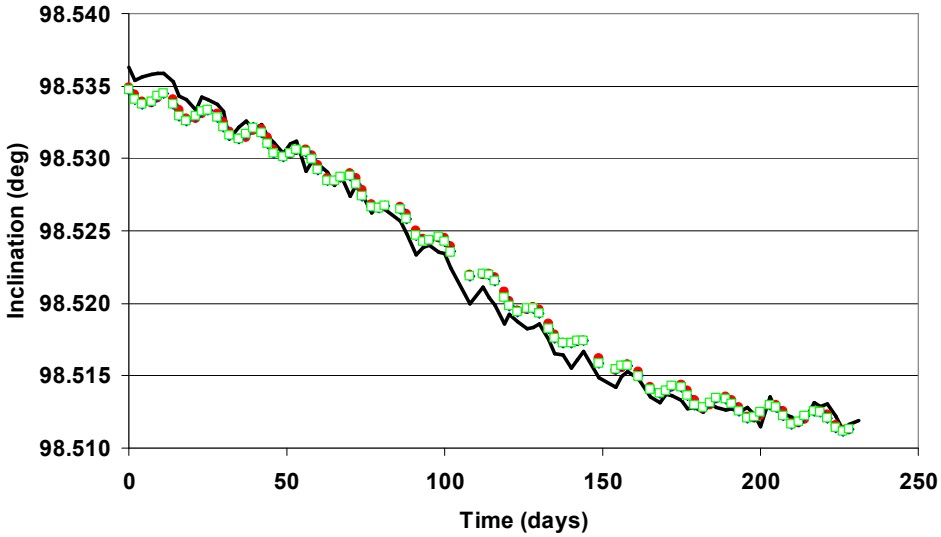

Figure 6. Orbit inclination of CBERS computed by CCS and numerical integration of drag

3.2. Solar Radiation Pressure Model Results

In this case, one shows the CCS semimajor axis and inclination mean elements against the proposed radiation pressure model, and the corresponding cannon ball models. That is, the cannon ball model results were included for fixed $C_r = 1.0$ and $C_r = 1.5$.

The inclusion of the radiation pressure perturbation in the numerical model provoked changes in the behavior of the orbital decay, as can be seen in Fig. 7. Although models with fixed coefficients had a good match around day 50, the numerical model (drag + radiation pressure) had better fit later around day 150. Similar to the drag case, it is difficult to figure a explanation to such difference between the models but one must investigate possibilities like that related to the positioning of the CBERS solar panel which moves following the Sun direction whereas this effect is not accounted for in fixed C_r models. The inclination evolution was also well matched for all models similar to the former case, shown in Fig. 6.

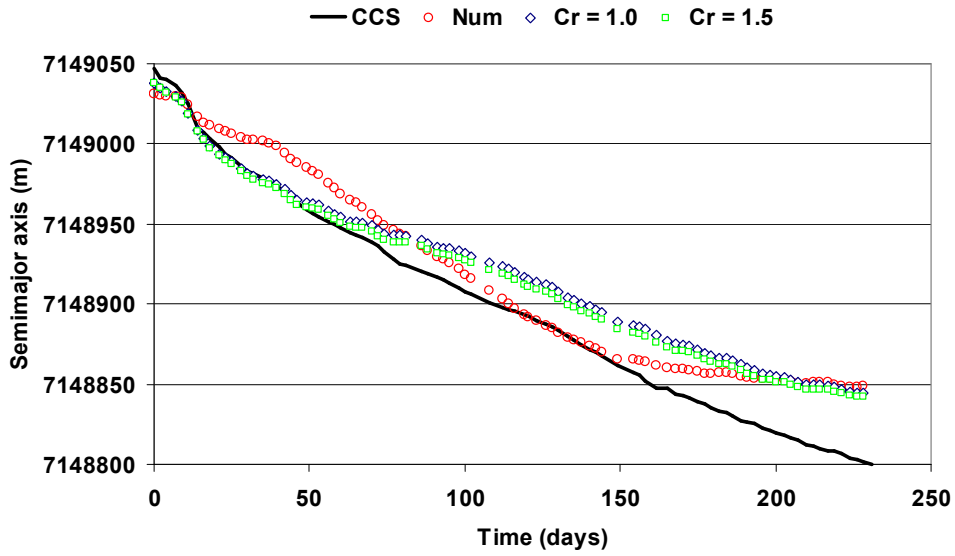

Figure 7. CBERS semimajor axis as computed by CCS and with numerical integration including solar radiation pressure

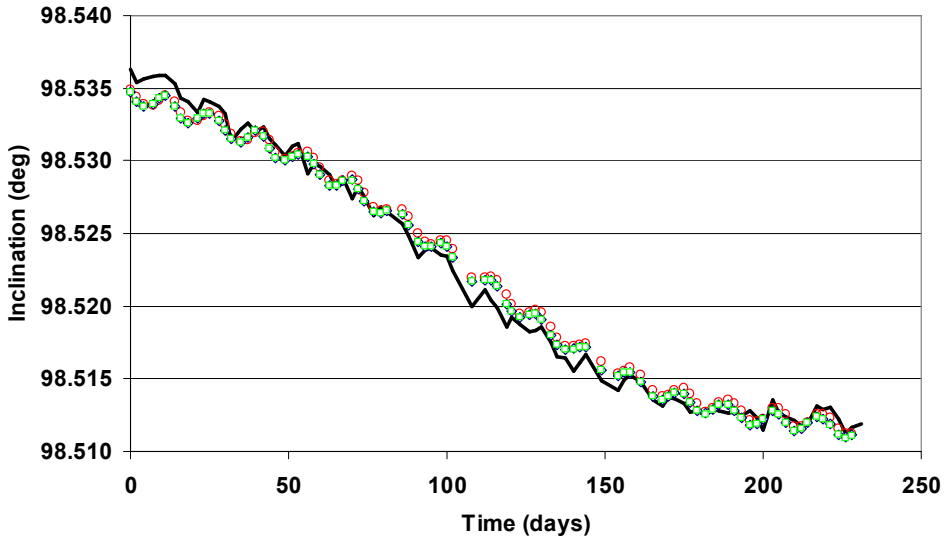

Figure 8. CBERS inclination as computed by CCS and with numerical integration including solar radiation pressure

3.3. Sun Moon Gravitational Attraction

In this section the CCS mean elements and the ones obtained from the proposed models of drag and radiation pressure, but disregarding the Sun and Moon point mass attraction were analyzed. It means that the perturbation due to Sun and Moon as a perturbing third body was not included in the numeric orbit integration. Figure 9 and 10 illustrates the importance of this perturbation, mainly in the inclination decay (Fig. 10). As expected the semimajor axis, shown in Fig. 9, is less affected by the gravitational perturbation of Sun and Moon. Besides the results had little difference from the former results. However the orbit inclination as shown in Fig. 10 did not decay because of the missing Sun and Moon perturbation.

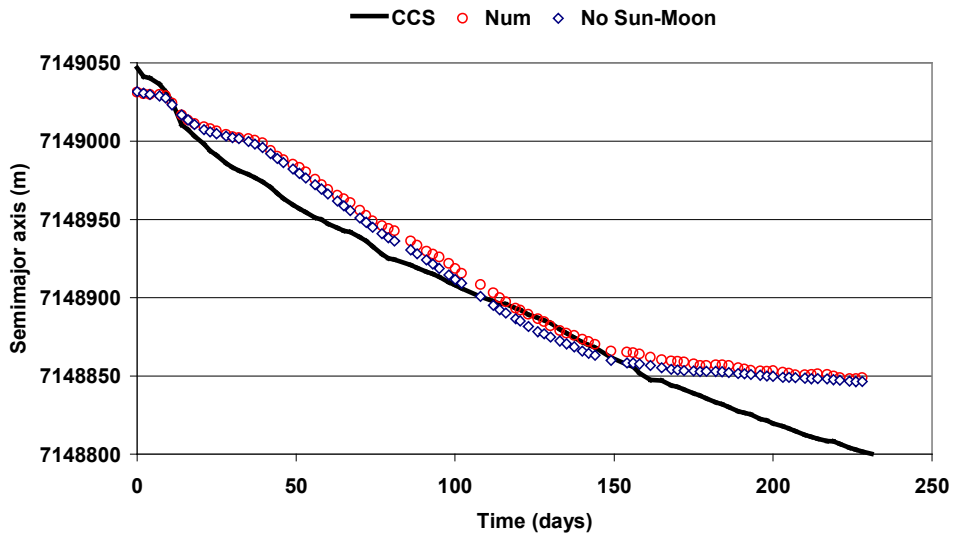

Figure 9. CBERS semimajor axis as computed by CCS and by numerical integration with and without Sun and Moon perturbations.

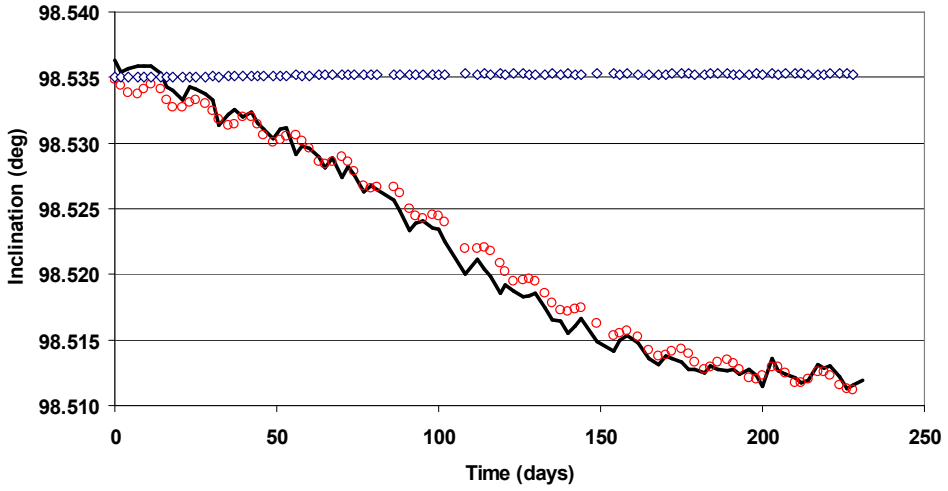

Figure 10. CBERS inclination as computed by CCS and by numerical integration with and without Sun and Moon perturbations.

6. Conclusions

This work realized an analysis of replacing the atmospheric drag and radiation pressure, which coefficients are conventionally considered constant, by a model which takes into account the satellite geometry. The analysis was performed on the basis of comparing the orbit elements (semimajor axis and inclination) between the methods (fixed coefficients and geometrical approach), with reference mean orbital data computed by the CBERS control center. Although the model using numerical integration of aerodynamics force and radiation pressure accounts for the effect of solar panel rotation, such effect is not pronounced in the results.

The orbital decay is strongly affected by the atmospheric density and this in turn is affected by the solar flux in the 10.7cm wavelength. The coupled effects make the methods, the numerical integration of forces on the satellite surface as well as the fixed coefficients (C_d and C_r) ones, to present similar results amongst them but differing to the actual reference orbit. The finding leads to the conclusion that the tabulated values for the solar flux and geomagnetic activity, to some extent, fail to reproduce faithfully the behavior of the satellite under the atmospheric drag. Nonetheless this numerical approach is promising as estimate of the drag effect to the attitude dynamics because the traditional approach of the displacement of the center of pressure clearly is not suited when the satellite has a complex geometrical shape.

With the approach proposed herein, the modeling of the aerodynamic forces can be customized to a specific satellite (in terms of its geometrical shape and material) and its nominal orbit. A complication here is the dependence with the solar activity (solar flux and geomagnetic indexes), which makes difficult to parameterize the model to work at any interval of solar cycle (11 years), without using the solar activity data. However, taking into account the nowadays micro-computer power, even with the current approach the computer burden was not compromised and the approach can be used with relatively short additional CPU times, at most 15%. For the radiation pressure, the geometry is easily taken into account and the customization is possible, as was already shown in [22]. Anyway the results have shown improvements in long term orbit prediction (e.g. some months). Taking into account that computing time is not a very constraining requirement (for off line tasks), it is expected that either the variable drag/radiation pressure coefficient on-line computation or a corresponding suitable empirical parameterization, e.g. [22] can be successfully applied in the upcoming CBERS missions.

7. References

[1] Schaaf, S. A. and Chambré, P. L. “Fundamentals of gas dynamics - high speed aerodynamics and jet propulsion. Vol III - Flow of rarefied gases”. Princeton, Princeton University Press, 1961. (Princeton Aeronautical Paperbacks, 8).

[2] Mueller, A. C. “Jacchia-Lineberry upper atmosphere density model”. Huston NASA, 1982. (NASA-CR-167824).

[3] Jacchia, L. G. “Thermospheric Temperature, Density and Compostion: New Models”. Cambridge, Ma, SAO, 1977. (SAO Special Report No 375).

[4] Wertz, J. R. “Spacecraft attitude determination and control”. D. Reidel Publishing, 1978.

[5] Present, R. D. “Kinetic Theory of Gases”. McGraw Hill, NY, 1958.

[6] Chapman, S. and Cowling, T. G. “The mathematical theory of Non-Uniform Gases”. 3. ed. Cambridge University Press, UK, 1970.

[7] Schamberg, R. “On Concave Bodies in Free Molecule Flow”. Rand Corporation, P-3164-1, 1967.

[8] Elliott, J. P. and Rasmussen, M. L. “Free-molecule Flow past a Cone”. AIAA Journal, Vol. 7, No. 1, 1969. pp. 78-86. doi: 10.2514/3.5038.

[9] Sentman L. H. and Karamcheti K. “Rarefied flow past a sphere”. AIAA Journal, Vol. 7, No. 1,1969. pp. 161-163. doi: 10.2514/3.5057.

[10] Cook, G. E. “The Aerodynamic Drag of Near Earth Satellites”. London: Her Majesty’s Stationary Office, 1960. C.P. No. 523.

[11] Stalder, J. R. and Zurick, V. J. “Theoretical aerodynamic characteristics of bodies in a free-molecule-flow field”. Washington, NACA, 1951. NACA Technical Note 2423.

[12] Carrara, V. “Satellite perturbation models” (in portuguese). São José dos Campos: INPE, 2013. 120 p. (sid.inpe.br/mtc-m19/2013/01.23.13.32-PUD). <http://urlib.net/8JMKD3MGP7W/3DE5SHE>.

[13] Carrara, V. “A (Huge) Collection of Interchangeable Empirical Models to Compute the Thermosphere Density, Temperature and Composition”. INPE-DMC, Available at <http://www2.dem.inpe.br/val/atmod/default.html>, 2011.

[14] NASA. “Spacecraft Radiation Torques”. NASA Space Vehicle Design Criteria (Guidance and Control). NASA SP-8027, 1969.

[15] Georgevic, R. M. “The solar radiation pressure force and torque model”. The Journal of the Astronautical Sciences, Vol. 20 No. 5, 1973. pp. 257-274.

[16] Knocke, P. C., Ries J. C. and Tapley B. D., “Earth Radiation Pressure Effects on Satellites”, Proceedings of the AIAA/ASS Astdodynamics Conference, (Washington, DC), AIAA Paper 88-4292, 1988. (doi: 10.2514/6.1988-4292).

[17] Carrara, V. “Environmental Disturbance Models (EDM) – User Manual” (in portuguese). São José dos Campos: INPE, 2013. 102 p. (sid.inpe.br/mtc-m19/2013/03.20.14.03-MAN). <http://urlib.net/8JMKD3MGP7W/3DP8Q6B>.

[18] Holmes, S.A.; Featherstone, W.E. “A unified approach to the Clenshaw summation and the recursive computation of very high degree and order normalised associated Legendre functions.” Journal of Geodesy, 76, p. 279-299, 2002.

[19] Kuga, H. K.; Carrara, V. “Fortran- and C-codes for higher order and degree geopotential and derivatives computation.” Proceedings of XVI SBSR - Brazilian Symposium on Remote Sensing, Iguassu Falls, Brazil, April 13-18, 2013, pp. 2201-2210. <www.dem.inpe.br/~hkk/software/high_geopot.htm>.

[20] Brouwer, D. “Solution of the problem of artificial satellite theory without drag.” The Astronomical Journal, V. 64, No. 1274, pp. 378-397, Nov. 1959.

[21] Fuming, Huang; Kuga, H. K. “CBERS simulator mathematical models.” Xian, China, XSCC (Xian Satellite Control Center), XSCC/INPE Internal Report CBTT/2000/MM/001, 1999.

[22] Ziebart, M. Generalized analytical solar radiation pressure modeling algorithm for spacecraft of complex shape. *Journal of Spacecraft and Rockets*, 41 (5), pp. 840-848, 2004.

9. Acknowledgements

The authors are grateful to the support from Brazilian Council for Scientific and Technological Development CNPq grant #303119/2010-1, and Foundation for Research of São Paulo State Fapesp grant #2012/21023-6.